JACS
JOURNAL OF THE AMERICAN CHEMICAL SOCIETY
Article
pubs.acs.org/JACS

Employing Forbidden Transitions as Qubits in a Nuclear Spin-Free Chromium Complex

Majed S. Fataftah, Joseph M. Zadrozny, Scott C. Coste, Michael J. Graham, Dylan M. Rogers, and Danna E. Freedman*

Department of Chemistry, Northwestern University, Evanston, Illinois 60208, United States

Supporting Information

ABSTRACT: The implementation of quantum computation (QC) would revolutionize scientific fields ranging from encryption to quantum simulation. One intuitive candidate for the smallest unit of a quantum computer, a qubit, is electronic spin. A prominent proposal for QC relies on high-spin magnetic molecules, where multiple transitions between the many M_S levels are employed as qubits. Yet, over a decade after the original notion, the exploitation of multiple transitions within a single manifold for QC remains unrealized in these high-spin species due to the challenge of accessing forbidden transitions. To create a proof-of-concept system, we synthesized the novel nuclear spin-free complex $[Cr(C_3S_5)_3]^{3-}$ with precisely tuned zero-field splitting parameters that create two spectroscopically addressable transitions, with one being a forbidden transition. Pulsed electron paramagnetic resonance (EPR) measurements enabled the investigation of the coherent lifetimes (T_2) and quantum control (Rabi oscillations) for two transitions, one allowed and one forbidden, within the $S = {}^3/_2$ spin manifold. This investigation represents a step forward in the development of high-spin species as a pathway to scalable QC systems within magnetic molecules.

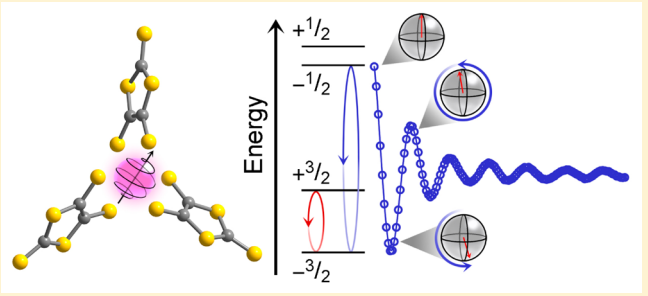

INTRODUCTION

The realization of quantum computation would transform fields from structural biology to quantum chemistry.[1] In principle, any two-level system that can be manipulated into a superposition of the two levels is a potential qubit, the fundamental unit of information in a quantum computer. Electronic spins, whereby qubits are realized from individual pairs of M_S levels and manipulated via microwave pulses,[2] are promising and intuitive candidates.[3−6] Fifteen years ago, high-spin molecules possessing a manifold of M_S levels were proposed as platforms for a specific implementation of quantum computation (QC).[7] The utility of high-spin molecules for QC lies in exploiting the manifold of states generated from a large ground-state spin split by axial (D) and transverse (E) zero-field splitting. Using such a system, a transition between each of the pairs of states could be used as a qubit. In this intricate approach, a single molecule could, in theory, serve as an entire computer. The investigation of species with these high-spin manifolds offers tremendous potential for creating multiple qubits in a single molecule, either by simultaneously accessing all transitions[7] or by creating discrete qubits.[5] The latter approach parallels and complements scalability induced by both hyperfine coupling and multinuclear complexes. The facile synthetic tunability of zero-field splitting parameters recommends these complexes as the ideal platforms for rational synthetic design. However, to date, experimental validations of the aforementioned proposal remain elusive.

Approaching the design and synthesis of a molecule suitable to achieve the foregoing proposal requires careful consideration of both the different energy levels involved and the stability of the qubits they host. This stability of the spin superpositions formed from pairs of M_S levels, or coherence time (T_2), is a particularly important figure of merit for qubit utility. One key challenge to housing multiple transitions within a single molecule arises from the difficulty in addressing forbidden transitions ($\Delta M_S \neq 1$) (Figure 1). One oft-employed creative approach sidesteps this challenge with larger molecular assemblies wherein multiple transitions are allowed by incorporating multiple spin centers.[8−14] Another highly successful approach employs mononuclear spin systems wherein hyperfine interactions create multiple accessible transitions.[15−18] Yet, the original scalability concept, which utilizes the zero-field splitting of a well-isolated spin ground state, remains elusive. Thus, progress toward the implementation of high-spin molecules for quantum computation lies in the detailed analyses of coherence and quantum control in multiple transitions. This effort crucially requires the study of weak, forbidden EPR transitions, as these form the bulk of the transitions utilized in the QC proposal of Leuenberger and Loss.[7]

High-spin transition metal molecules with appreciable zero-field splitting represent arguably the most tunable approach to

Received: November 10, 2015
Published: January 7, 2016

DOI: 10.1021/jacs.5b11802
J. Am. Chem. Soc. 2016, 138, 1344−1348

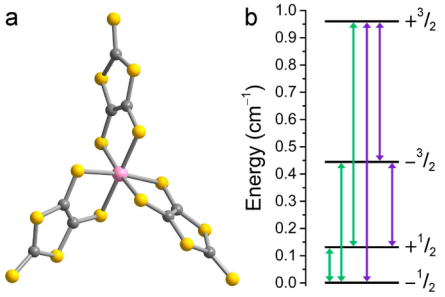

Figure 1. (a) Molecular structure of $[Cr(C_3S_5)_3]^{3-}$ as found in the crystal structure of **1**. Pink, yellow, and gray spheres represent Cr, S, and C atoms, respectively. Selected interatomic distances (Å) and angles (deg): Cr−S_{ave}, 2.4158(8); S−Cr−$S_{bite,ave}$, 87.76(3); and S−Cr−S_{others}, 88.26(1). (b) Calculated splitting of the M_S energy levels of **1** with H_{dc} = 2000 G aligned along the *z*-axis of the molecule, with D = +0.260 cm^{-1} and E = −0.080 cm^{-1} (parameters determined from 51.6 GHz EPR experiments, *vide infra*). The arrows illustrate the three allowed (green) and three forbidden (purple) transitions within the S = $^3/_2$ manifold.

qubit design. Here, we exploit this tunability to enable the manipulation of a forbidden transition as a qubit. This serves as a vital proof of concept to demonstrate the potential for creating multiple qubits in a single molecule. To engender multiple spectroscopically addressable transitions on a commercial spectrometer, the design of a molecule with a small |*D*| is imperative. This small |*D*|, as depicted in Figure 1, allows multiple transitions to be accessed within the spectral window. Furthermore, we note that few of the numerous theoretically accessible transitions within a spin manifold are typically addressable based on EPR spectroscopic selection rules ($\Delta M_S = \pm 1$). Relaxation of these selection rules thus opens up the possibility of observing resonances that otherwise display negligible transition intensity. Any interaction that causes the M_S levels to mix intensifies a forbidden EPR transition. Common interactions responsible for mixing are anisotropic interionic exchange coupling, hyperfine interactions, or zero-field splitting.[19−22] However, exchange and hyperfine interactions can be highly detrimental to the stability of the superposition in multinuclear qubits. Furthermore, large zero-field splitting in mononuclear high-spin systems can engender fast spin−lattice relaxation (T_1) times, inherently limiting T_2.[23] Owing to these factors, in addition to the difficulty in observing formally forbidden transitions in molecules possessing low rhombicity (E/D),[24] we targeted relatively simple, mononuclear complexes with low magnetic anisotropy and a high E/D. We hypothesized that these two specific properties would afford highly mixed M_S levels at low magnetic fields, which would produce significant intensity of forbidden EPR transitions for study. Toward this end, we designed and synthesized a novel d^3 pseudo-octahedral nuclear spin-free species of chromium(III), $[Cr(C_3S_5)_3]^{3-}$ (Figure 1). The tendency toward rhombic distortion and low axial zero-field splitting observed in hexacoordinate complexes of this ion[25] recommended it as ideal to produce forbidden transitions. Note that the absence of nuclear spin within the complex both reduces nuclear spin-mediated decoherence and prevents hyperfine coupling from complicating spectral interpretation, allowing assignment of the transitions as originating purely from the electronic spin. Herein, we report the new complex $[Cr(C_3S_5)_3]^{3-}$ and demonstrate the control of two transitions, one allowed and one formally forbidden, within its ground-state spin manifold.

RESULTS AND DISCUSSION

The targeted compound $(Ph_4P)_3[Cr(C_3S_5)_3]$ (**1**) was synthesized by treatment of $CrCl_3(THF)_3$ with 3 equiv of $Na_2(C_3S_5)$ in methanol and isolated via precipitation with 3 equiv of $(Ph_4P)Br$. Single-crystal X-ray diffraction experiments revealed a trigonally distorted pseudo-octahedral chromium(III) ion bound by three bidentate $C_3S_5^{2-}$ ligands (Figure 1a). The ligands in this complex are composed of only carbon and sulfur atoms, elements that possess >98% natural abundances of nuclear spin-free isotopes. Furthermore, chromium itself possesses 90.4% natural abundance of nuclear spin-free isotopes combined with an extremely low magnetic moment of $-0.474\mu_N$ for its spin active I = $^3/_2$ isotope. Thus, **1** is a member of a growing class of molecules specifically designed to be nuclear spin-free.[16,24,26−29]

Our investigation of the viability of **1** as a qubit began with the elucidation of its M_S-level manifold using magnetometry and continuous-wave (cw) EPR spectroscopy. Variable-temperature dc magnetic susceptibility data from 1.8 to 300 K and H_{dc} = 1000 G revealed $\chi_M T$ = 1.84 cm^3 K/mol at 300 K, close to the 1.875 cm^3 K/mol expected for a S = $^3/_2$ chromium(III) ion (see Figures S1−S3). With decreasing temperature, the value of $\chi_M T$ remains relatively constant, but it decreases below 10 K, owing to zero-field splitting. We probed **1** via X-band (~9.7 GHz) and 51.6 GHz cw-EPR spectroscopy to precisely quantitate the magnitude and sign of the apparent zero-field splitting (Figures 2 and S4). The observed spectra were modeled with the program EASYSPIN[30] and the spin Hamiltonian $\hat{H} = D\hat{S}_z^2 + E(\hat{S}_x^2 - \hat{S}_y^2) + \Sigma g_i\mu_B \boldsymbol{HS}$, which provides the energies of the M_S levels for the spin $\boldsymbol{S}$ as a function of axial (D) and transverse (E) zero-field splitting parameters as well as the applied dc magnetic field ($\boldsymbol{H}$). In this Hamiltonian, $\hat{S}_i^2$ ($i = x, y$, and z) are the spin operators, g_i ($i = x$, y, and z), the g factors, and μ_B, the Bohr magneton. We were able to simulate both spectra and determine the parameters D = 0.326(8) cm^{-1}, E = −0.107(5) cm^{-1}, g_x = 1.99(2), g_y = 2.02(5), and g_z = 1.96(7) from the X-band spectrum. These values are consistent with those obtained from the 5 K, 51.6 GHz spectrum (Figure S4). Here, slight differences between the magnitudes of the g, D, and E values at 298 K versus 5 K are likely due to a slight temperature dependence of the spin Hamiltonian parameters.[31] Nevertheless, the values are within the expected range of octahedral chromium(III) species and are in agreement with the magnetic susceptibility data (see Figure S3). The determined rhombicity E/D here (0.31) is near the maximal limit (0.33), which importantly heralds highly mixed M_S levels. The small, positive D value predicts a set of M_S = $\pm^1/_2$, $^3/_2$ doublets split by only 0.52 cm^{-1} at H_{dc} = 0 G (Figures 2 and S5). The relative scale of this splitting versus the X-band (~9.7 GHz, 0.32 cm^{-1}) quantum and the highly mixed M_S levels suggest that **1** appears to be perfectly in line with our design criteria and readily suited to afford multiple M_S pairs for investigation.

We employed pulsed X-band EPR spectroscopy to evaluate the suitability of **1** as a platform for multiple electron spin-based qubits. Owing to the deleterious effects that accompany interactions between an electronic spin qubit and surrounding electronic and nuclear spins, all pulsed EPR analyses were performed on a dilution of $(d^{20}\text{-}Ph_4P)_3[Cr(C_3S_5)_3]$ with $(d^{20}\text{-}Ph_4P)_3[Ga(C_3S_5)_3]$, $(d^{20}\text{-}Ph_4P)_3[Cr_{0.01}Ga_{0.99}(C_3S_5)_3]$ (**1′**). First, the intensity of the Hahn-echo for **1′** following a set of two microwave pulses ($^\pi/_2 - \tau - \pi - \tau -$ echo) was monitored

DOI: 10.1021/jacs.5b11802
J. Am. Chem. Soc. 2016, 138, 1344−1348

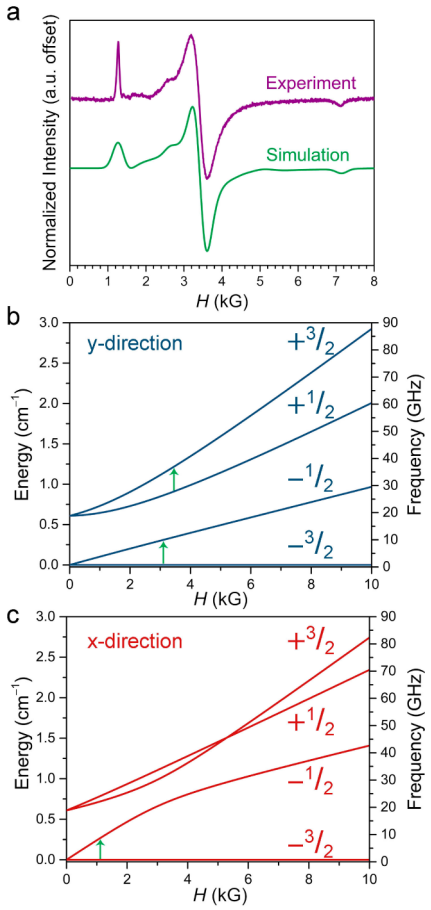

Figure 2. (a) 298 K X-band (9.45 GHz) cw-EPR spectrum for **1**. The green line is a simulated spectrum with g_x = 1.99(2), g_y = 2.02(5), g_z = 1.96(7), D = +0.326(8) cm^{-1}, and E = −0.107(5) cm^{-1}. (b) Zeeman energy level diagram for a magnetic field alignment along the y direction, where green arrows highlight the origin of the central transition at 3500 G observed in the EDFS spectrum for **1**′.[32] (c) Energy level diagram for a magnetic field alignment along the y direction. Over the range of H_{dc} = 0 to 6000 G, the M_S = $+^3/_2$ level is highly mixed with the M_S = $-^1/_2$ level.[32] The green arrow highlights the $\pm^3/_2$ intra-Kramers transition as the origin of the peak at 1000 G in the EDFS spectrum of **1**′. Energies for panels b and c are normalized to the energy of the ground M_S = $-^3/_2$ level, and the energies are calculated with the spin Hamiltonian parameters determined from the X-band analysis.

as a function of applied dc magnetic field. The resultant echo-detected, field-swept EPR spectrum (EDFS) reveals an intense transition at H_{dc} = 3500 G and a second, weaker peak at H_{dc} = 1000 G (see Figure S6), corresponding to those observed in the cw-EPR spectrum of Figure 2a. A nonzero echo intensity in the EDFS indicates the presence of an EPR transition, but, moreover, the ability of the given pair of M_S levels to form a superposition on a measurable time scale. Thus, the observation of two different peaks in the EDFS reveals two separate pairs of M_S levels for investigation in $[Cr(C_3S_5)_3]^{3-}$.

Zeeman diagrams constructed on the basis of the cw-EPR analyses (see Figures 2 and S5) reveal the parentage of the EPR transitions, and we note that the identity of the M_S levels has important implications on the control and stability for a given spin system.[2,32] Note that application of a magnetic field along the z-axis of a molecule with a positive D yields an M_S = $\pm^1/_2$ pair stabilized by $|2D|$ relative to the M_S = $\pm^3/_2$ pair. However, if the field is aligned along the x,y axes of the molecule, then the Zeeman diagram appears noticeably different. For the x alignment, the lowest energy M_S levels are the $\pm^3/_2$ levels, whereas M_S level assignment for the y-aligned Zeeman diagram is very difficult to intuit at low field owing to extensive mixing. Inspection of these diagrams indicates that all signals seen in the X-band EDFS derive intensity from the ground M_S = $-^3/_2$ level. The intense H_{dc} = 3500 G peak obtains most of its intensity from the y component of the inter-Kramers M_S = $-^3/_2$ → M_S = $-^1/_2$ transition at 5 K, with a small contribution from the excited M_S = $+^1/_2$ → M_S = $+^3/_2$ resonance. The significantly weaker signal at 1000 G, in contrast, arises from the M_S = $-^3/_2$ → M_S = $+^3/_2$ ground-state intra-Kramers transition. Note that this latter resonance, with ΔM_S = 3, is formally forbidden by EPR selection rules (ΔM_S = 1). However, the energy gaps between the M_S levels in $[Cr(C_3S_5)_3]^{3-}$ are quite small owing to the small D and low magnetic field. Because the M_S levels for **1** are so close in energy, appreciable mixing of the M_S = $+^3/_2$ and M_S = $-^1/_2$ levels is induced by the large rhombicity, a fact evident by the broad avoided-crossing zones in Figure 2b,c. This M_S level mixing induces a relaxation of the ΔM_S = ±1 selection rule and consequently appreciable intensity for the forbidden transition.

The lifetimes of the superpositions, commonly denoted as spin−spin relaxation times (T_2) or coherence times, were next determined for the two peaks revealed in the EDFS. These parameters are extracted from modeling the decay of the intensity of the two-pulse Hahn-echo sequence with increasing interpulse delay time τ (see Figures 3 and S7). A plot of the

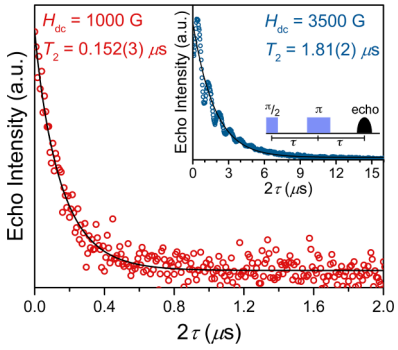

Figure 3. Hahn-echo decay curves for **1**′ at 5 K. Data were collected at H_{dc} = 1000 (red circles) and 3500 G (blue circles, inset). Black lines represent best fits of the decay curves to stretched exponential decays with T_2 = 1.81(2) μs and 152(3) ns at H_{dc} = 3500 and 1000 G, respectively. The 2.2 MHz oscillation detected in the 3500 G data is due to deuterium ESEEM (see the Supporting Information).

echo intensity of **1**′ as a function of 2τ reveals an exponentially decaying signal with increasing delay time at both peaks in the EDFS. Fits of stretched exponential decay functions to the 5 K echo intensity data yield T_2 = 1.81(3) and 0.152(2) μs at 3500 and 1000 G, respectively (see Figures 3, S7, and S8). The former value is within the observed range of other transition metal complexes,[23,33−35] whereas the low-field T_2 is comparably short.

Preliminary studies of the mechanisms of superposition collapse, which contribute to the process known as decoherence, proceeded in **1**′ via comparison of the T_2 data with the spin−lattice relaxation times (T_1). The magnitude of T_1 represents an upper limit for the magnitude of T_2. Therefore, T_1 ∼ T_2 when decoherence is driven by thermal

DOI: 10.1021/jacs.5b11802
J. Am. Chem. Soc. 2016, 138, 1344−1348

and vibrational effects. T_1 was determined for **1′** by inversion recovery ($\pi - T - {}^{\pi}/_{2} - \tau - \pi - \tau -$ echo) experiments (see Figures S9–S11). At 5 K, the values of T_1 for the low- and high-field resonances are 47(5) μs and 29(3) ms, respectively, which are several orders of magnitude higher than the observed T_2 values. With increasing temperature, the magnitude of T_1 at the main resonance drops from 29(3) ms at 5 K to 875(5) μs at 30 K. In concert, T_2 at the main resonance drops only 1 μs in value, from 1.81(3) μs at 5 K to 0.82(2) μs at 30 K. The relative magnitude of T_1 to T_2 over the entire investigated temperature range suggests that T_2 is not T_1-limited. Thus, we hypothesize that the ^{2}D (I = 1) and ^{31}P ($I = {}^{1}/_{2}$, 100% natural abundance) nuclear spins of the $(d_{20}\text{-Ph}_4\text{P})^+$ counterions and ^{69}Ga and ^{71}Ga ($I = {}^{3}/_{2}$, 99.92% natural abundance) nuclei are the most important mediators of decoherence here.

The ability to drive an electronic spin into any arbitrary superposition of a given pair of M_S levels is a key quality of a candidate qubit. The two peaks in the EDFS, as well as their analysis by inspection of the Zeeman diagrams, offered the enticing possibility to evaluate the qubit candidacy of the two separate transitions within the spin manifold for $[Cr(C_3S_5)_3]^{3-}$. Echo detected nutation experiments were performed at the two resonances detected in the EDFS (see Figures 4 and S12–S16) to assess qubit viability. In these experiments, a microwave nutation pulse, also known as a tipping pulse, is applied to drive the spin into a superposition of the two M_S levels of a given resonance. A suitable spin qubit will be cycled through all arbitrary superpositions of its two constituent M_S levels with increasing nutation pulse length, which yields a smooth oscillation in the detected signal, known as a Rabi oscillation. As displayed in Figure 4, Rabi oscillations are detected at both 3500 and 1000 G for **1′**, an observation that establishes the viability of each of these transitions for potential quantum control. The dependence of the frequency of the oscillation, the Rabi frequency (Ω_R), on B_1 is expected to be linear if the oscillation arises from driving the spin between two M_S levels, as opposed to a cavity background signal.[11] Fourier transformation of the nutation data (see Figure S13 and S16) reveals a linear dependence of Ω_R on B_1 (see Figure 4b), which establishes with certainty the provenance of the nutations and is consistent with other transition metal complexes studied for QIP.[9−11,26−29,32,33,35−38]

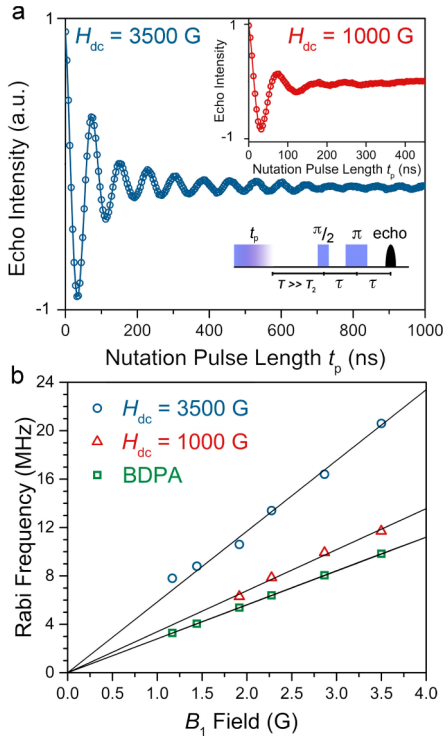

Figure 4. (a) Rabi oscillations at H_{dc} = 3500 and 1000 G and Rabi frequency dependence on B_1. Data were collected at H_{dc} = 3500 G (blue circles), B_1 = 2.3 G and at H_{dc} = 1000 G, B_1 = 3.5 G (red circles, inset) at T = 5 K. Solid lines connecting the data points are guides for the eye. (b) Rabi frequency plotted as a function of increasing B_1 for **1′** and BDPA. The black lines are best fits to the data with slopes of 5.85(1), 3.24(2), and 2.8 MHz/G for the 3500 and 1000 G data sets and that of BDPA, respectively. The marked difference of the slopes is indicative of control over different pairs of M_S levels.

The Rabi frequency yields an experimental time scale for one of the simplest operations in a spin qubit, the spin-flip ($\Omega_R = (2\tau_{spin\text{-}flip})^{-1}$. At 3500 and 1000 G and B_1 = 3.5 G, $\tau_{spinflip}$ is 12 and 16 ns, respectively. These observations highlight one of the key advantages of electronic spin-based quantum computation: rapid operation time. Indeed, achieving a T_2 of merely milliseconds enables the execution of thousands of operations, a requisite condition for performing actual computations.[39] A particularly exciting aspect of this parameter is its dependence on tunable properties of the spin. For example, the Ω_R for a given oscillation displays a B_1 dependence governed by the M_S levels of the probed transition and the g-factor of the spin center.[2,40] The strongly differing B_1 dependences of Ω_R for **1′**, 5.85(1) and 3.24(2) MHz/G, respectively, for the 1000 and 3500 G resonances, therefore, reflects the involvement of different M_S levels in the two transitions, as suggested by our assignment of the EDFS. Crucially, the complex displays stronger B_1 dependence at both transitions than the $M_S = -{}^{1}/_{2} \rightarrow M_S = +{}^{1}/_{2}$ transition of the $S = {}^{1}/_{2}$ 1,3-bisdiphenylene-2-phenylallyl radical (BDPA; Figure 4b). These results and others[29] illustrate the utility of molecular fine-tuning in high-spin species as a strategy to decreasing spin-flip operation times.

OUTLOOK

The successful design of a single molecule that displays allowed and forbidden resonances available for study is a modest step toward realizing the proposal made by Leuenberger and Loss for high-spin molecules over a decade ago.[7] The foregoing results detail our utilization of the tunability of mononuclear transition metal complexes to enable the investigation of both forbidden and allowed EPR transitions in the context of QC. Importantly, this ability permitted the study of the control of separate resonances, wherein we demonstrate enhancement of the Rabi frequency by nearly a factor of 2 over a radical system through inclusion of higher M_S levels in the EPR resonance. Together with recent demonstrations of long coherence times in molecular species,[27,28,37,38] these properties imbue considerable promise to coordination complex-based qubits. Our investigation of the qubit candidacy of allowed and forbidden transitions in the same molecule further suggests new directions for synthetic chemistry, wherein species are designed explicitly for the relaxation of EPR selection rules. The foregoing results represent initial steps toward new qubit platforms that will enable future studies of qubit scalability within single-molecule hosts.[7]

DOI: 10.1021/jacs.5b11802
J. Am. Chem. Soc. 2016, 138, 1344−1348

■ ASSOCIATED CONTENT

Supporting Information

The Supporting Information is available free of charge on the ACS Publications website at DOI: 10.1021/jacs.5b11802.

Full experimental section and methods; additional spectroscopic, crystallographic, and magnetic data (PDF)

Crystallographic data for **1** (CIF)

Crystallographic data for **2** (CIF)

■ AUTHOR INFORMATION

Corresponding Author

*danna.freedman@northwestern.edu

Notes

The authors declare no competing financial interest.

■ ACKNOWLEDGMENTS

We thank Mr. Samuel Greer, Ms. Lakshmi Bhaskaran, and Drs. J. van Tol, A. Ozarowski, L. Song, and Prof. S. Hill for fruitful discussions and experimental assistance. We are grateful for the financial support of Northwestern University, The Institute for Sustainability and Energy at Northwestern University (ISEN) Booster Award number 10031846, and the National Science Foundation for CAREER award no. 1455017. Work at the NHMFL is supported by the NSF (DMR-1157490) and the State of Florida.

■ REFERENCES

(1) Nielson, A. M.; Chuang, I. L. *Quantum Computation and Quantum Information*; Cambridge Universal Press: Cambridge, 2010.

(2) Schweiger, A.; Jeschke, G. *Principles of Pulsed Magnetic Resonance*; Oxford University Press: New York, 2001.

(3) Cerletti, V.; Coish, W. A.; Gywat, O.; Loss, D. *Nanotechnology* **2005**, *16*, R27−R49.

(4) Awschalom, D. D.; Bassett, L. C.; Dzurak, A. S.; Hu, E. L.; Petta, J. R. *Science* **2013**, *339*, 1174−1179.

(5) Aromí, G.; Aguilà, D.; Gamez, P.; Luis, F.; Roubeau, O. *Chem. Soc. Rev.* **2012**, *41*, 537−546.

(6) Ochsenbein, S. T.; Gamelin, D. R. *Nat. Nanotechnol.* **2011**, *6*, 112−115.

(7) Leuenberger, M. N.; Loss, D. *Nature* **2001**, *410*, 789−793.

(8) Ardavan, A.; Rival, O.; Morton, J. J. L.; Blundell, S. J.; Tyryshkin, A. M.; Timco, G. A.; Winpenny, R. E. P. *Phys. Rev. Lett.* **2007**, *98*, 057201.

(9) Bertaina, S.; Gambarelli, S.; Mitra, T.; Tsukerblat, B.; Müller, A.; Barbara, N. *Nature* **2008**, *453*, 203−206.

(10) Choi, K.-Y.; Wang, Z.; Nojiri, H.; van Tol, J.; Kumar, P.; Lemmens, P.; Bassil, B. S.; Kortz, U.; Dalal, N. S. *Phys. Rev. Lett.* **2012**, *108*, 067206.

(11) Yang, J.; Wang, Y.; Wang, Z.; Rong, X.; Duan, C.-K.; Su, J.-H.; Du, J. *Phys. Rev. Lett.* **2012**, *108*, 230501.

(12) Aguilà, D.; Barrios, L. A.; Velasco, V.; Roubeau, O.; Repollés, A.; Alonso, P. J.; Sesé, J.; Teat, S. J.; Luis, F.; Aromí, G. *J. Am. Chem. Soc.* **2014**, *136*, 14215−14222.

(13) Timco, G. A.; Carretta, S.; Troiani, F.; Tuna, F.; Pritchard, R. J.; Muryn, C. A.; McInnes, E. J. L.; Ghirri, A.; Candini, A.; Santini, P.; Amoretti, G.; Affronte, M.; Winpenny, R. E. P. *Nat. Nanotechnol.* **2009**, *4*, 173−178.

(14) Nakazawa, S.; Nishida, S.; Ise, T.; Yoshino, T.; Mori, N.; Rahimi, R.; Sato, K.; Morita, Y.; Toyota, K.; Shiomi, D.; Kitagawa, M.; Hara, H.; Carl, P.; Hoefer, P.; Takui, T. *Angew. Chem., Int. Ed.* **2012**, *51*, 9860−9864.

(15) Bertaina, S.; Gambarelli, S.; Tkachuk, A.; Kurkin, I. N.; Malkin, B.; Stepanov, A.; Barbara, B. *Nat. Nanotechnol.* **2007**, *2*, 39−42.

(16) Zadrozny, J. M.; Niklas, J.; Poluektov, O. G.; Freedman, D. E. *J. Am. Chem. Soc.* **2014**, *136*, 15841−15844.

(17) Ghosh, S.; Datta, S.; Friend, L.; Cardona-Serra, S.; Gaita-Ariño, A.; Coronado, E.; Hill, S. *Dalton Trans.* **2012**, *41*, 13697−13704.

(18) Ueda, A.; Suzuki, S.; Yoshida, K.; Fukui, K.; Sato, K.; Takui, T.; Nakasuji, K.; Morita, Y. *Angew. Chem., Int. Ed.* **2013**, *52*, 4795−4799.

(19) Abragam, A.; Bleaney, B. *Electron Paramagnetic Resonance of Transition Ions*; Dover Publications, Inc.: New York, 1986.

(20) Boča, R. *Theoretical Foundations of Molecular Magnetism, Current Methods in Inorganic Chemistry*; Elsevier Science: Amsterdam, 1999; Vol. *1*.

(21) Datta, S.; Waldmann, O.; Kent, A. D.; Milway, V. A.; Thompson, L. K.; Hill, S. *Phys. Rev. B* **2007**, *76*, 052407.

(22) Gatteschi, D.; Sessoli, R. *Angew. Chem., Int. Ed.* **2003**, *42*, 268−297.

(23) Eaton, S. S.; Eaton, G. R. *Biol. Magn. Reson.* **2002**, *19*, 29−129.

(24) Fataftah, M. S.; Zadrozny, J. M.; Rogers, D. M.; Freedman, D. E. *Inorg. Chem.* **2014**, *53*, 10716−10721.

(25) Bonomo, R. P.; Di Bilio, A. J.; Riggi, F. *Chem. Phys.* **1991**, *151*, 323−333.

(26) Graham, M. J.; Zadrozny, J. M.; Shiddiq, M.; Anderson, J. S.; Fataftah, M. S.; Hill, S.; Freedman, D. E. *J. Am. Chem. Soc.* **2014**, *136*, 7623−7626.

(27) Bader, K.; Dengler, D.; Lenz, S.; Endeward, B.; Jiang, S.-D.; Neugebauer, P.; van Slageren, J. *Nat. Commun.* **2014**, *5*, 5304.

(28) Zadrozny, J. M.; Niklas, J.; Poluektov, O. G.; Freedman, D. E. *ACS Cent. Sci.* **2015**, *1*, 488−492.

(29) Zadrozny, J. M.; Freedman, D. E. *Inorg. Chem.* **2015**, *54*, 12027−12031.

(30) Stoll, S.; Schweiger, A. *J. Magn. Reson.* **2006**, *178*, 42−55.

(31) Corzilius, B.; Michaelis, V. K.; Penzel, S. A.; Ravera, E.; Smith, A. A.; Luchinat, C.; Griffin, R. G. *J. Am. Chem. Soc.* **2014**, *136*, 11716−11727.

(32) For simplicity, our labeling scheme for the M_S levels in Figures 2 and S5 employs the labels that correspond to the high-field limit, where the M_S levels are pure.

(33) Schlegel, C.; van Slageren, J.; Manoli, M.; Brechin, E. K.; Dressel, M. *Phys. Rev. Lett.* **2008**, *101*, 147203.

(34) Moro, F.; Kaminski, D.; Tuna, F.; Whitehead, G. F. S.; Timco, G. A.; Collison, D.; Winpenny, R. E. P.; Ardavan, A.; McInnes, E. J. L. *Chem. Commun.* **2014**, *50*, 91−93.

(35) Wedge, C. J.; Timco, G. A.; Spielberg, E. T.; George, R. E.; Tuna, F.; Rigby, S.; McInnes, E. J. L.; Winpenny, R. E. P.; Blundell, S. J.; Ardavan, A. *Phys. Rev. Lett.* **2012**, *108*, 107204.

(36) Baldoví, J. J.; Cardona-Serra, S.; Clemente-Juan, J. M.; Coronado, E.; Gaita-Ariño, A.; Prima-García, H. *Chem. Commun.* **2013**, *49*, 8922−8925.

(37) Warner, M.; Din, S.; Tupitsyn, I. S.; Morley, G. W.; Stoneham, A. M.; Gardener, J. A.; Wu, Z.; Fisher, A. J.; Heutz, S.; Kay, C. W. M.; Aeppli, G. *Nature* **2013**, *503*, 504−508.

(38) Tesi, L.; Lucaccini, E.; Cimatti, I.; Perfetti, M.; Mannini, M.; Atzori, M.; Morra, E.; Chiesa, M.; Caneschi, A.; Sorace, L.; Sessoli, R. *Chem. Sci.* **2016**, Advance Article. DOI: 10.1039/C5SC04295J.

(39) DiVincenzo, D. P. *Fortschr. Phys.* **2000**, *48*, 771−783.

(40) Stoll, S.; Jeschke, G.; Willer, M.; Schweiger, A. *J. Magn. Reson.* **1998**, *130*, 86−96.

DOI: 10.1021/jacs.5b11802
J. Am. Chem. Soc. 2016, 138, 1344−1348